

Supporting Information

Synergy in photomagnetic/ferromagnetic *sub*-50 nm core-multishell nanoparticles

Nada Dia,^{‡,§} Laurent Lisnard,^{*,‡} Yoann Prado,^{‡ ||} Alexandre Gloter,[¶] Odile Stéphan,[¶] François Brisset,[‡] Hala Hafez,[§] Zeinab Saad,[§] Corine Mathonière,^{*,†} Laure Catala,^{*,‡} and Talal Mallah[‡]

[‡] *Institut de Chimie Moléculaire et des Matériaux d'Orsay, rue du Doyen Poitou, Université Paris Sud 11, 91405 Orsay, France.*

^{||} *Institut Parisien de Chimie Moléculaire, UMR CNRS 7201, UPMC Univ Paris 06, 4 Place Jussieu, 75005 Paris, France.*

[¶] *Laboratoire de Physique des Solides, UMR 8502, Université Paris-Sud 11, F-91405 Orsay, France.*

[§] *Ecole Doctorale des Sciences et de Technologie, Hadath campus P.O.Box 5, Université Libanaise Beyrouth, Liban.*

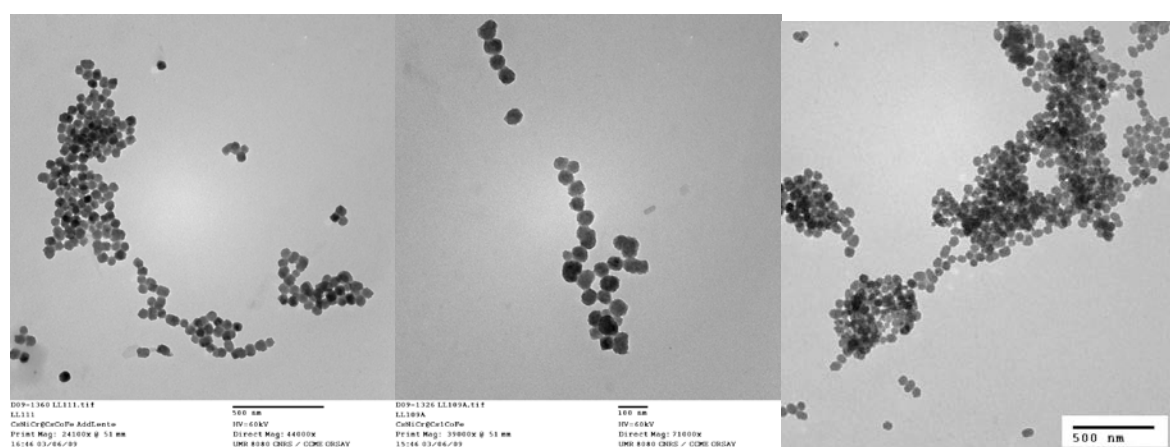
[†] *Institut de Chimie de la Matière Condensée de Bordeaux UPR 9048, 87 avenue du Dr Albert Schweitzer, Pessac, F-33608, France.*

Additional comments on the synthesis of 2Cs and 3Cs

To ensure optimum conditions we varied the amount of caesium ion used for the preparation of the CoFe shell between 0 and 2 equivalents of $\text{Cs}/\text{Co}^{\text{II}}$.

Indeed high ionic forces in the synthesis media may trigger side nucleation. As pH adjustment (and therefore increased ionic force) is required to prevent the formation of $\text{Co}^{\text{II}}-\text{CN}-\text{Fe}^{\text{II}}$ pairs we sought to decrease the ionic force through a diminishing of the amount of added caesium ions. Keeping in mind that we in parallel wish to reach a sufficient insertion of alkali ions in the CoFe shell to lead predominant $\text{Co}^{\text{III}}-\text{Fe}^{\text{II}}$ pairs, the growth of the CsCoFe shell has been performed for various amounts of Cs^+ ions. We have found that the best compromise between controlled growth and $\text{Co}^{\text{III}}-\text{Fe}^{\text{II}}$ predominance have been obtained for 0.4 equivalent of Cs^+ ion per divalent metal ion. This represents the lowest amount of alkali ions one can add to keep a maximum of inserted Cs^+ .

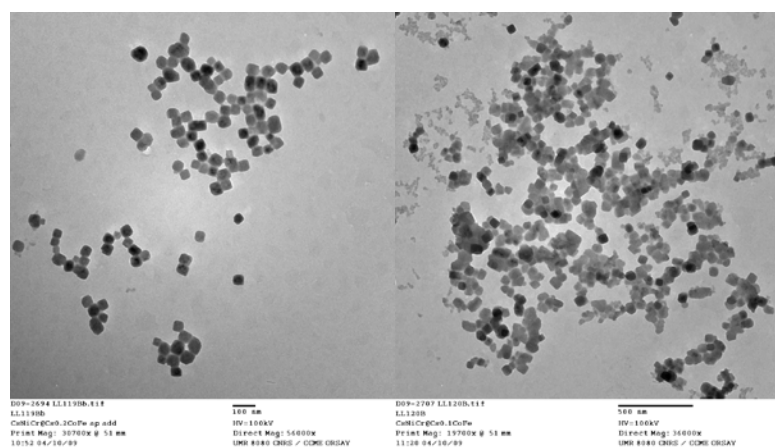
Some TEM images and UV-visible absorption spectra have been added to illustrate the effect of the various amounts of Cs^+ as shown below.



2 equivalents of $\text{Cs}^+/\text{Co}^{2+}$

1 equivalent of $\text{Cs}^+/\text{Co}^{2+}$

0.5 equivalent of $\text{Cs}^+/\text{Co}^{2+}$



0.2 equivalent of $\text{Cs}^+/\text{Co}^{2+}$

0.1 equivalent of $\text{Cs}^+/\text{Co}^{2+}$

Fig S1a. TEM micrographs of the CsNiCr@CsCoFe samples prepared with different amounts of Cs^+ . TEM images show a rather good control while the roughness is lower for smaller amounts of Cs^+ .

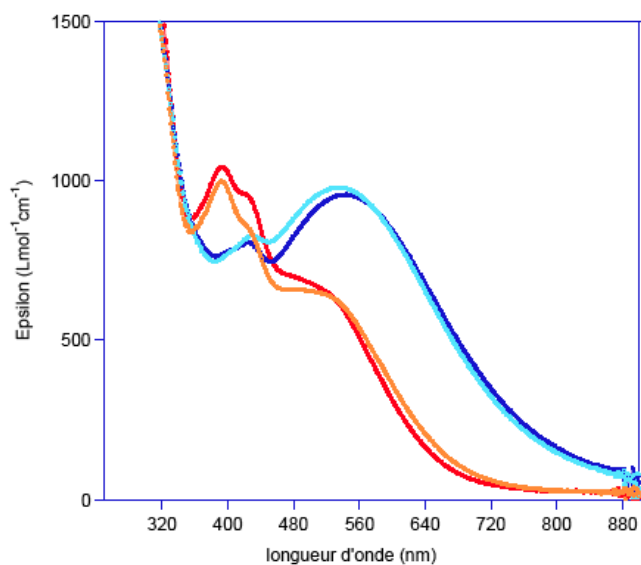


Figure S1b. UV-visible absorption spectra of different samples prepared with 0 eq (red curve), at 0.2 eq (yellow curve), 0.4 eq (light blue curve) and 2 equivalents (dark blue curve)

The UV-visible absorption spectra have been measured for varying amounts of Cs⁺ (in eq. per divalent metal ion), and it was found that the predominance of the Co^{II}-Fe^{III} state is reached for 0.2 equivalent of Cs⁺ while the Co^{III}-Fe^{II} state is obtained for 0.4 and 2 equivalents of Cs⁺.

Hence the best compromise found was 0.4 equivalent of Cs⁺ to achieve the convenient Cs⁺ insertion while avoiding an excess of alkali in the remaining solution.

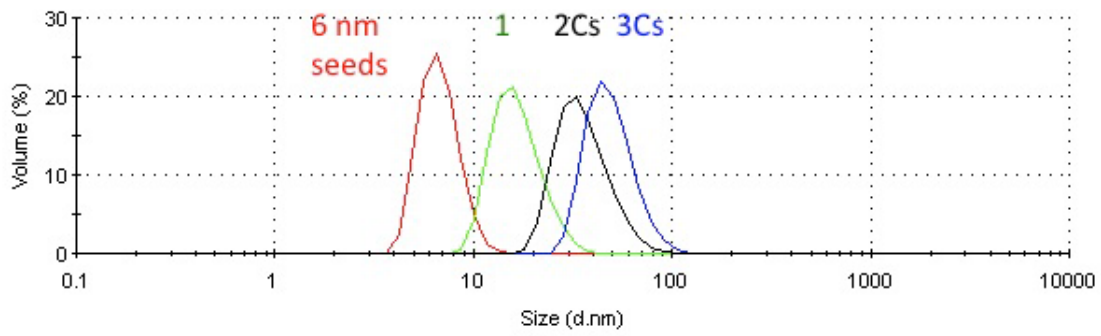


Figure S2. Dynamic light scattering of aqueous colloidal solutions of 6 nm CsNiCr seeds (red), CsNiCr cores, **1** (green), **2Cs** (black) and **3** (blue)

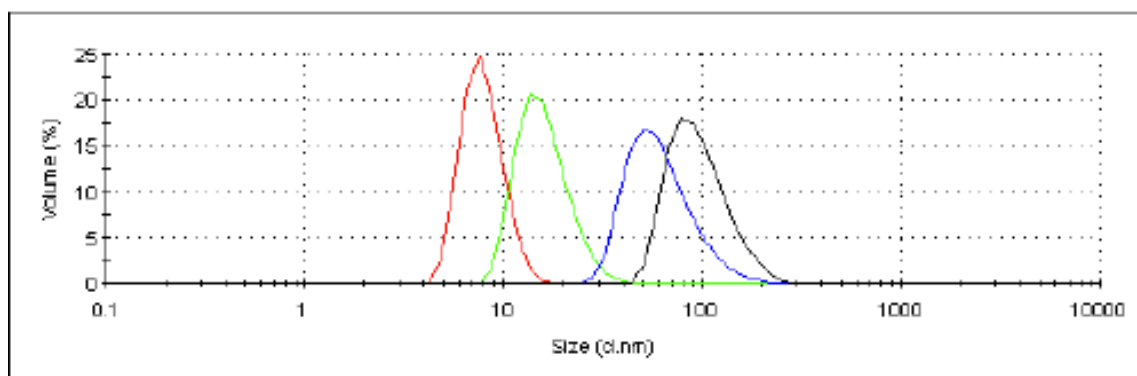


Figure S3a. Dynamic light scattering of aqueous colloidal solutions of 6 nm seeds (red) **1** (green), **2** (blue) and **3** (black)

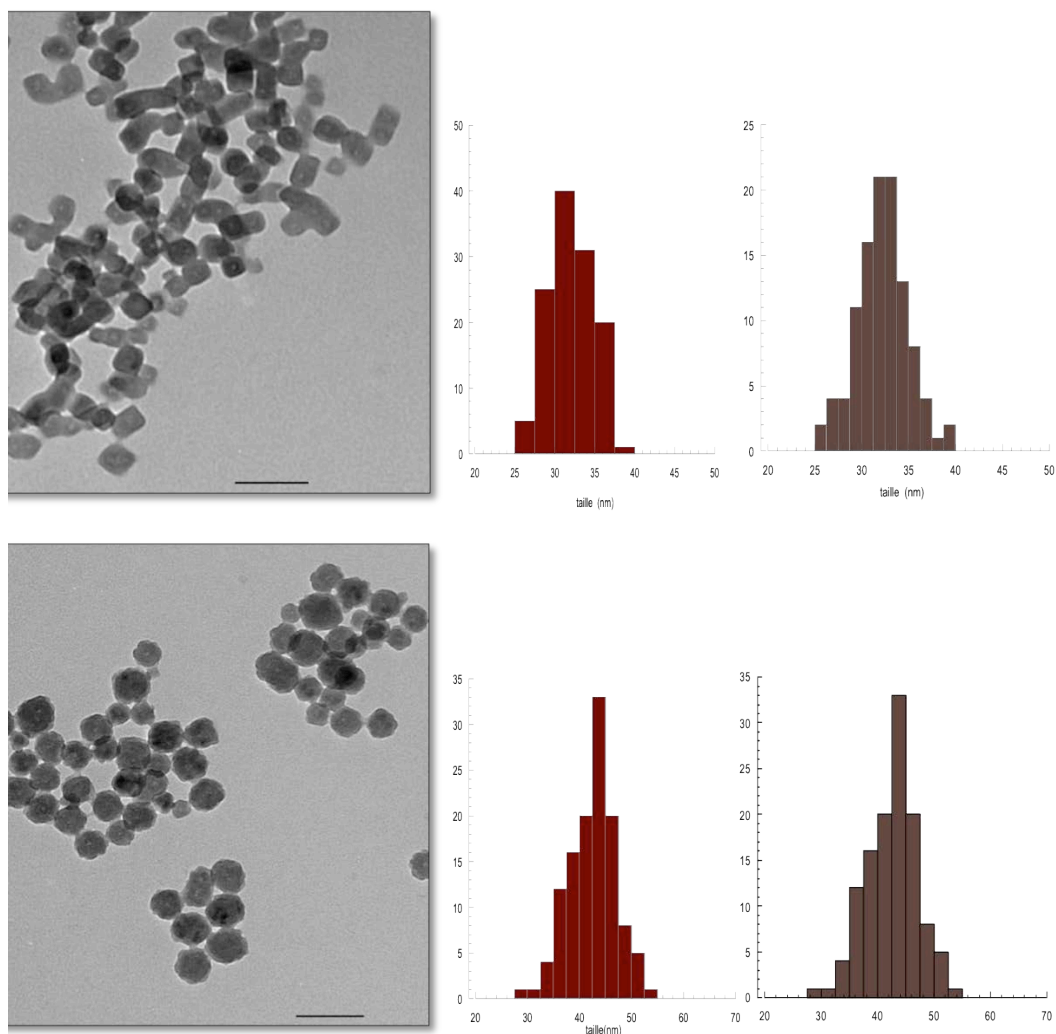


Figure S3b. TEM images and size distribution diagrams (length and width) for **2** (top) and **2Cs** (bottom). Scale bar : 100 nm.

Table S1. Energy dispersive X-ray spectroscopy.

% atomic element	2Cs	3Cs	2	3
Cs	21.8	22.3	6.1	16.2
Ni	2.2	24.4	2.6	26.6
Cr	2.2	17.4	2.5	16.5
Co	41.5	18.3	51.8	20.9
Fe	32.3	17.5	37.2	19.7

To provide the reader with a fairly good representation of the composition of each compound, a step-by-step determination by EDS analysis has been performed.

These formulae are not only based on EDS measurements, but also C, H N elemental analysis and charge balance considerations. Knowing the composition of the core by full elemental analysis it is possible using the EDS metal ratios to determine the compositions of each shell, in a stepwise manner. Indeed, in the synthesis, **3** is grown on **2** which is grown on **1** (the same goes for **3Cs** and **2Cs**). Therefore, knowing the composition of **1**, the EDS measurements on **2** give access to the composition of the CoFe shell in **2** and in **3**. The EDS measurements on **3** give then the CsNiCr shell composition. Samples **2** and **3**, as well as **2Cs** and **3Cs** have been isolated from the same synthesis batch for all these analysis. These ratios have been checked on a second batch of samples independently.

Preliminary experiments :

To reduce the amount of NiFe pairs located at the interface, we have performed the synthesis introducing 0.8 eq of ferricyanide during the (Cs)CoFe shell growth and performed the EDS analysis, that confirms the good control of the heterostructure growth.

Table S2. Energy dispersive X-ray spectroscopy

% atomic element	CsNiCr@CsCoFe	CsNiCr@CsCoFe@CsNiCr	CsNiCr@CoFe	CsNiCr@CoFe@CsNiCr
Cs	1.9	16.8	21.0	23.3
Ni	2.8	24.3	2.6	23
2Cr	2.7	20.2	2.5	21.4
Co	45.6	18.8	51.8	16.4
Fe	37.7	15.6	37.2	13.1

The compositions calculated for the inorganic cores are :

When CsCl is introduced during the first shell growth :



When no CsCl is introduced in the first shell growth



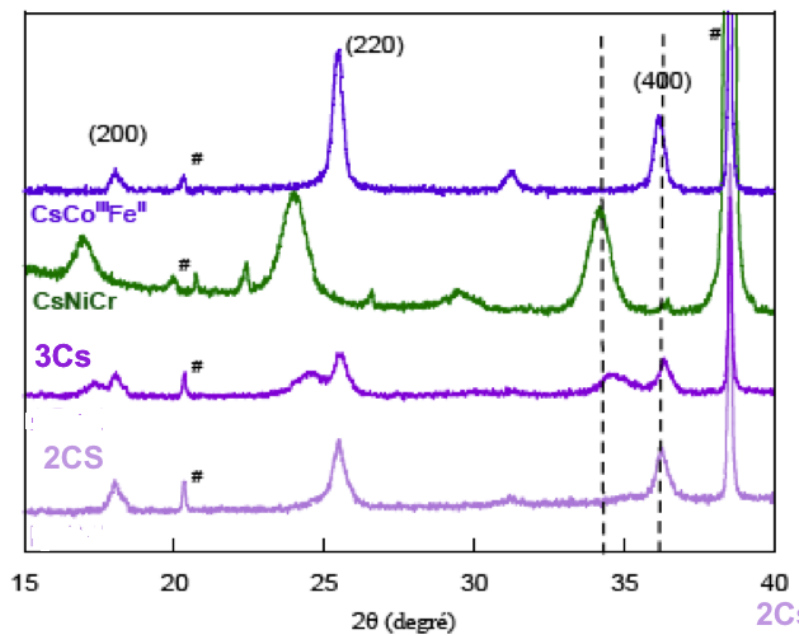


Figure S4. X-ray powder patterns of **3Cs**, **2Cs** and pure CsNiCr , $\text{CsCo}^{\text{III}}\text{Fe}^{\text{II}}$ nanoparticles. Peaks marked with # come from the aluminium sample holder.

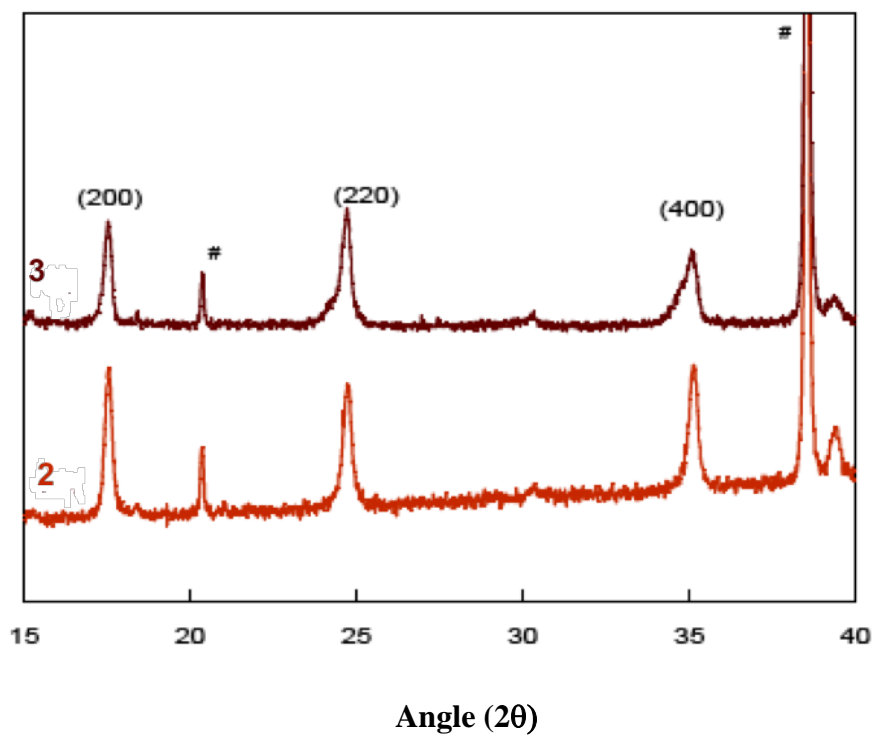


Figure S5. X-ray powder patterns of **2** and **3**. Peaks marked with # come from the aluminium sample holder.

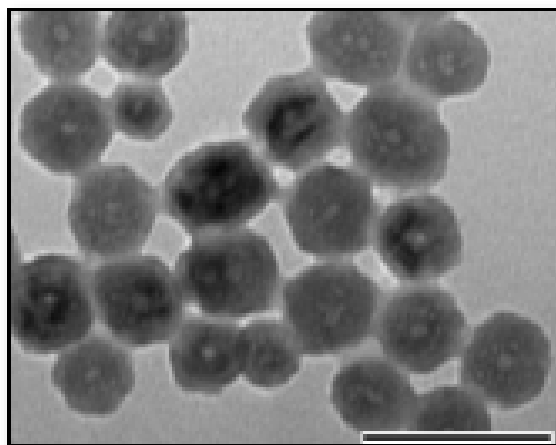
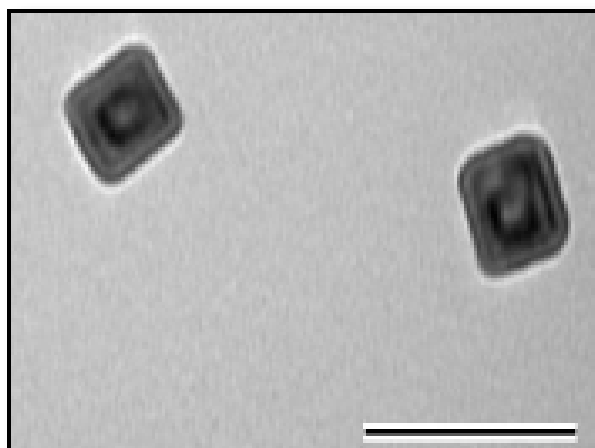


Figure S6 Transmission electron microscopy on **3** and **3Cs** (scale bar 100 nm).

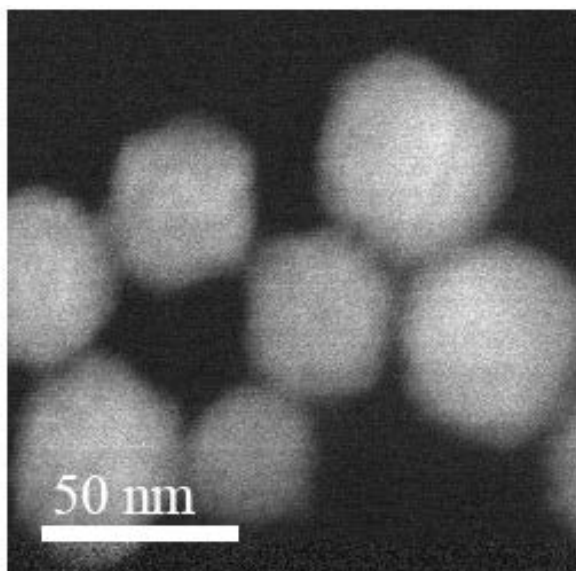
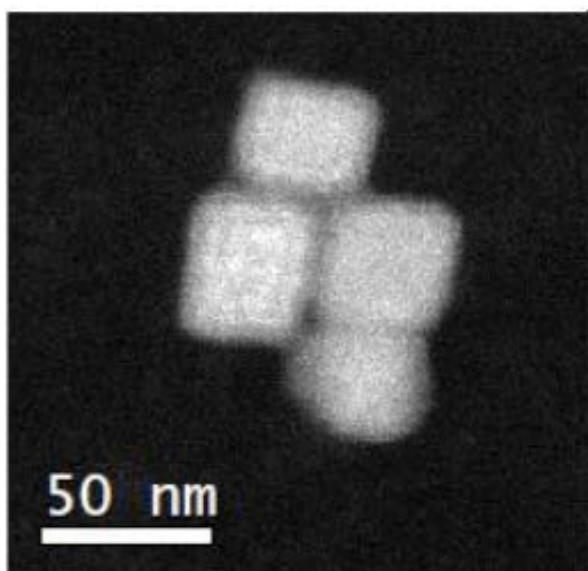


Figure S7. High angular dark field scanning transmission electron microscopy (HAADF-STEM) images of on **3** and **3Cs**.

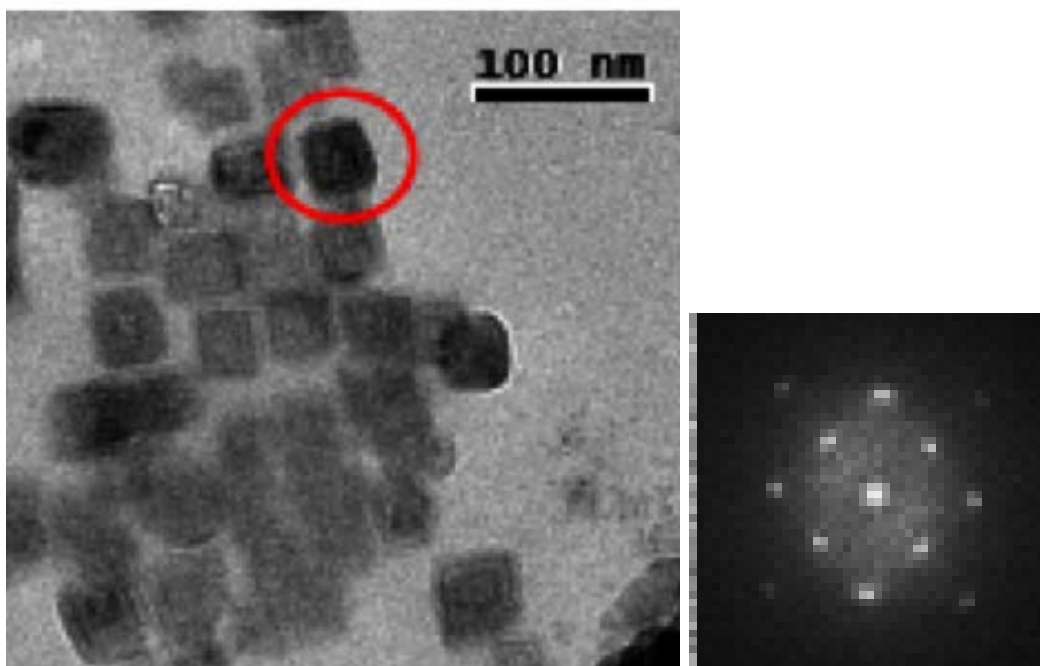


Figure S8. High resolution transmission electron microscopy of **3** with electronic diffraction pattern.

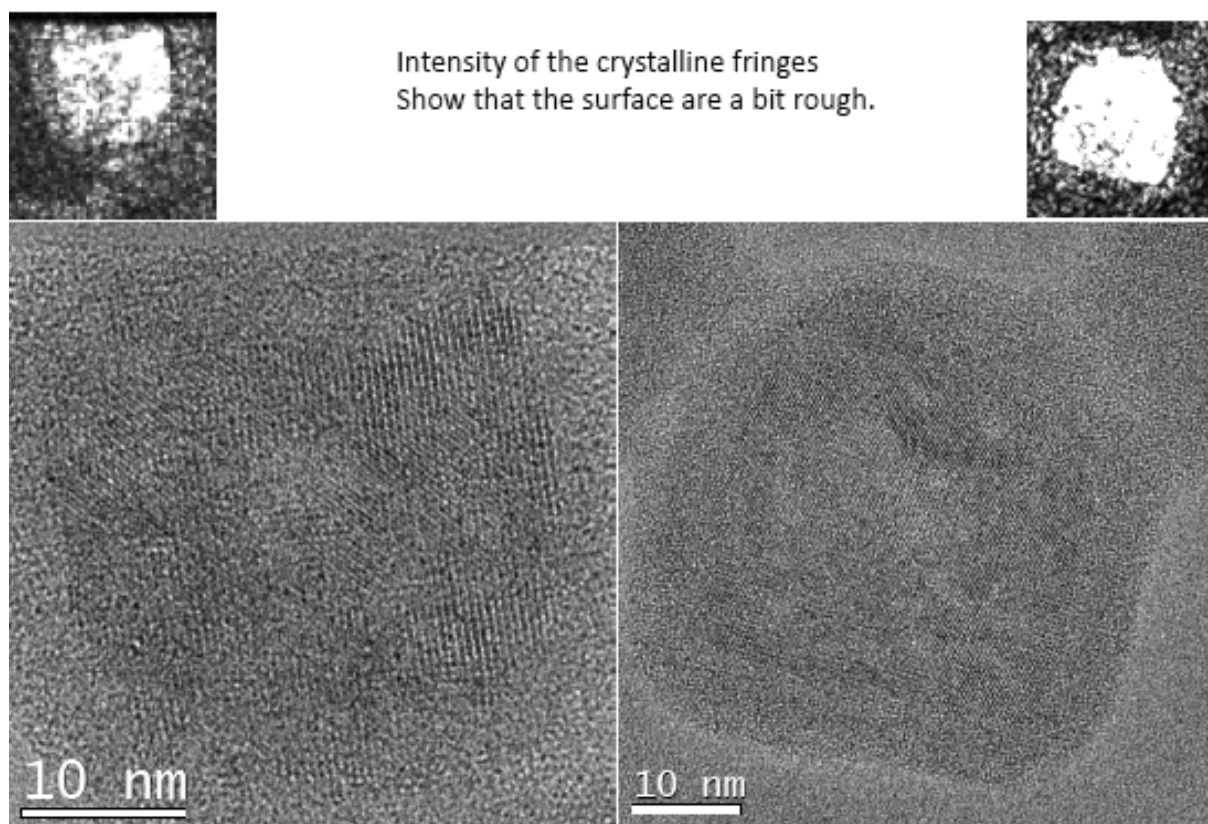


Figure S9. High resolution Transmission Electron Microscopy of two particles of **3Cs**.

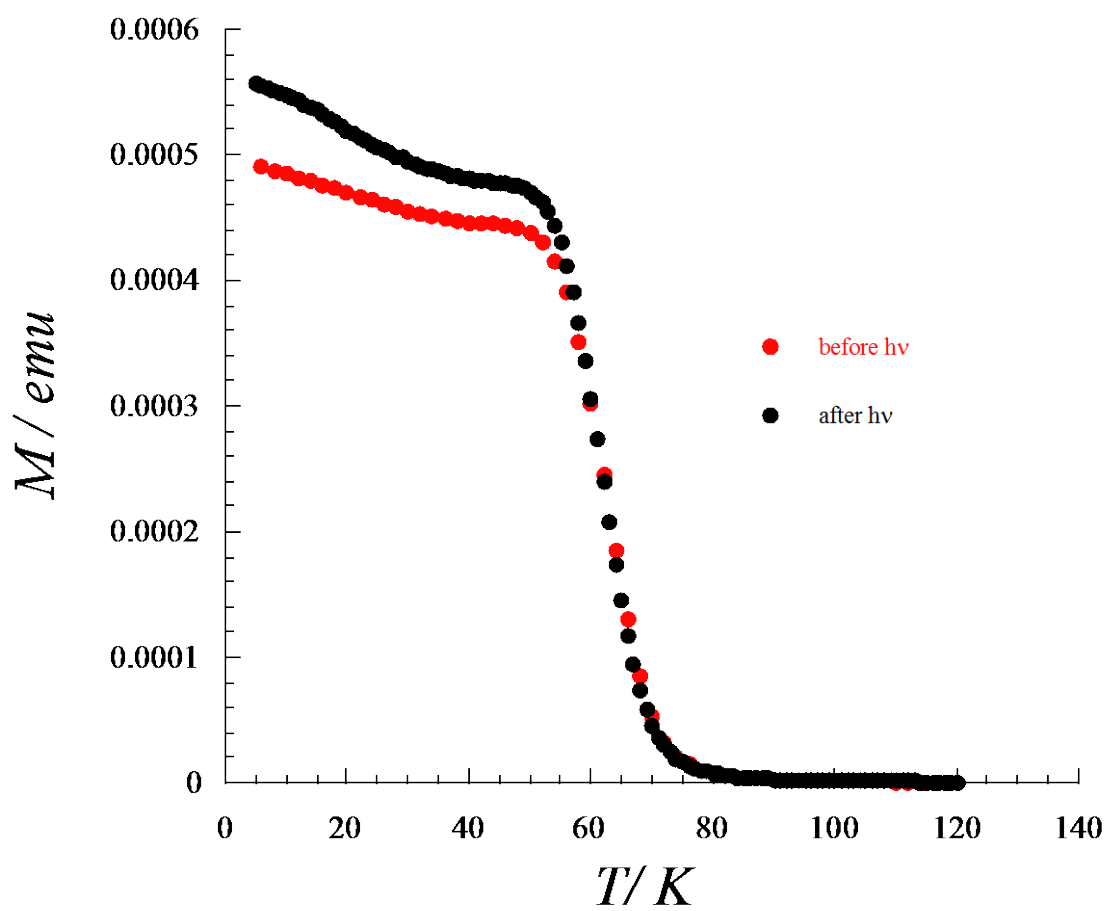


Figure S10. Evolution of the FC magnetization of 3Cs recovered with CTA⁺ before and after irradiation.

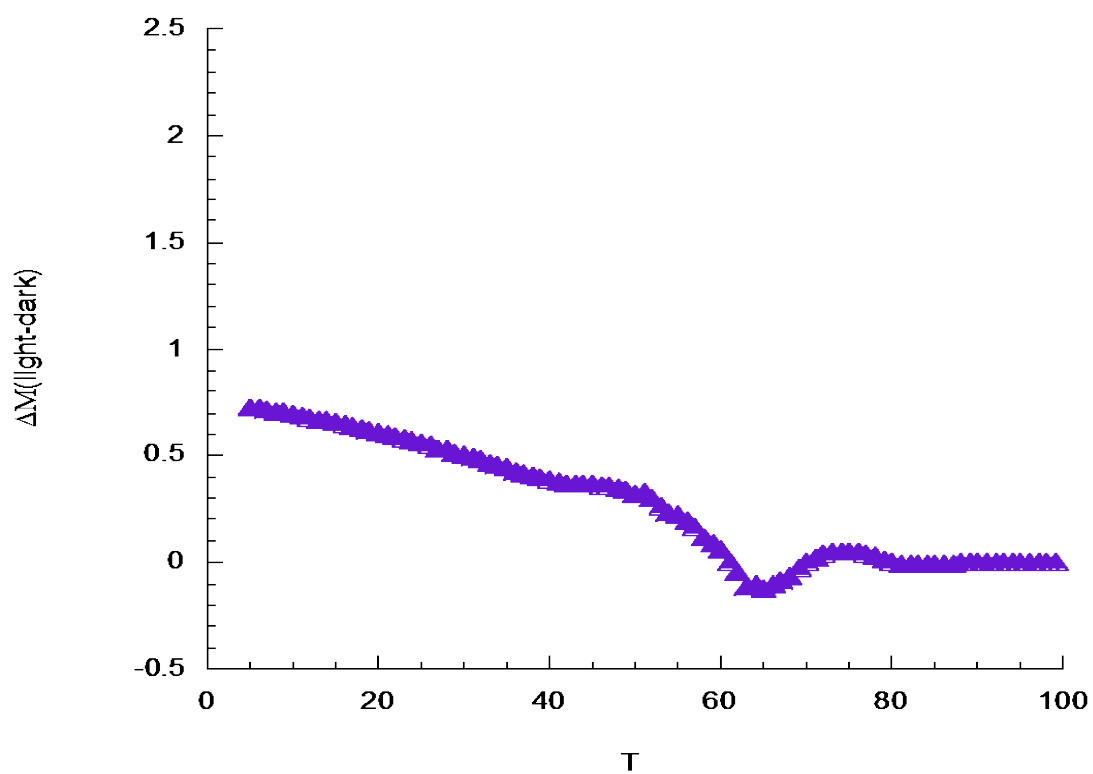


Figure S11. Difference between the FC magnetizations after and before light irradiation, showing that the positive value drops down to zero at 60 K.